Morphology and chemical composition of Taiwan oil millet (Eccoilopus formosanus) epicuticular wax

Marita Anggarani, Yu-Ying Lin, Shao-An Fang, Hshin-Ping Wu, Chi-Chih Wu, Wann-Neng Jane, Thomas James Roscoe, Frédéric Domergue, Yue-Ie Caroline Hsing

ORIGINAL ARTICLE

Morphology and chemical composition of Taiwan oil millet (*Eccoilopus formosanus*) epicuticular wax

Marita Anggarani[1], Yu-Ying Lin[1], Shao-An Fang[1], Hshin-Ping Wu[1], Chi-Chih Wu[1], Wann-Neng Jane[1], Thomas James Roscoe[2], Frederic Domergue[3] and Yue-Ie Caroline Hsing[1*]

[1]Institute of Plant and Microbial Biology, Academia Sinica, 128 Sec. 2 Academia Rd., Nangang, Taipei, 115201 Taiwan.

[2]Regulations Epigenetiques et Developpement de la Graine, ERL 5300 CNRS-IRD UMR DIADE, IRD Centre de Montpellier, 911 Avenue Agropolis, 34394 Montpellier, France

[3]Univ. Bordeaux, CNRS, LBM, UMR 5200, F-33140 Villenave d'Ornon, France

Corresponding author

Yue-Ie Caroline Hsing

Email: bohsing@gate.sinica.edu.tw

Phone: +886-2-2787-1170

Abstract

Main Conclusion **Taiwan oil millet has two types of epicuticular wax: platelet wax composed of alcohols and filament wax constituted primarily by the singular compound of C_{28} free fatty acids.**

Abstract Taiwan oil millet (TOM–*Eccoilopus formosanus*) is an orphan crop cultivated by the Taiwan indigenous people. It has conspicuous white powder covering its leaf sheath indicating the abundance of epicuticular waxes, thus may contribute to its resilience. Here, we characterized the epicuticular wax secretion in TOM leaf blade and leaf sheath using various microscopy techniques, as well as gas chromatography to determine its composition. Two kinds of waxes, platelet and filaments, were secreted in both the leaf blades and sheaths. The platelet wax is secreted ubiquitously by epidermal cells, whereas the filament wax is secreted by a specific epidermal cell called cork cells. The newly developed filament waxes were markedly re-synthesized by the cork cells through the papillae protrusions on the external periclinal cell wall. The predominant wax component was a C_{28} primary alcohol in leaf blade, and a C_{28} free fatty acid in the leaf sheath, pseudopetiole and midrib. The wax morphology present in distinct organ and abundance corresponds to the specific chemical composition: platelet wax composed of alcohols exists mainly in the leaf blade, whereas filament wax constituted mainly by the singular compound of C_{28} free fatty acids is present abundantly in leaf sheath. Our study clarifies the filament wax composition in comparison to previous study in sorghum. Both platelet and filament waxes comprise a protection barrier for TOM.

Key words: cork cell, epicuticular wax, epidermal cell, filament wax, Taiwan oil millet (*Eccoilopus formosanus*), wax composition.

INTRODUCTION

Taiwan oil millet (TOM–*Eccoilopus formosanus* (Rendle) A. Camus) is a semi-domesticated crop that is classified in the genus of *Eccoilopus* together with its wild counterpart, *E. cotulifer*. It is a perennial plant that is mainly cultivated by indigenous people of Taiwan as one of their staple crops. TOM was first identified by Rendle (Henry 1904) and is preserved in the Kew Royal Botanic Gardens (Kew 2022). TOM plant has been largely ignored in the recent decades, yet a few indigenous people continue to cultivate and consume it as part of their culture (Takei 2013). TOM is the sole endemic grain crop in Taiwan so that we are interested to assess any potential of this semi-domesticated crop for its agronomic and nutritional benefits, particularly as a way to increase agri-diversity. Older classifications identified TOM as *Spodiopogon formosanus,* and its closest relative, based on the available literature, is *S. sibiricus,* a frost grass that is more primitive than *Andropogon gerardii* according to grass phylogenetics using three chloroplast markers (Grass Phylogeny Working 2012). *S. sibiricus* is within the tribe of Andropogoneae and subfamily of Panicoideae, together with sugarcane, sorghum, and maize. However, more recent classification have placed this *Spodiopogon* (*Eccoilopus*) in the subtribe Andropogoninae, separate from the subtribe Saccharinae, which includes sorghum, sugarcane, and silver grass (*Miscanthus*) (Soreng et al. 2017). The Taiwanese name for this plant is “oil miscanthus” instead of “oil millet”. That is because oil millet plant morphology is more similar to miscanthus, while its seeds have a similar size to foxtail millet (Chen et al. submitted).

Plant cuticular waxes are typically a complex mixture of hydrophobic compounds such as very long chain fatty acids, hydrocarbons (or alkanes), alcohols, aldehydes, esters, triterpenes, sterols and flavonoids (Post-Beittenmiller 1996). Epicuticular waxes are present on the plant surface, while intracuticular waxes are embedded in the cutin polymer matrix (Koch et al. 2004). The composition of cuticular waxes varies among and within plant species due to the differences among organs and tissues, and across developmental stages (Post-Beittenmiller 1996). Major functions for the plant cuticle include controlling transpiration as well as polar solutes, gas and vapor exchanges (Riederer 2006). The plant cuticle also minimizes the effects of UV radiation, and also serves as an interface for biotic interactions. For example, a reduced amount of epicuticular wax and

cuticle deposition in sorghum made it more susceptible to fungal infection (Jenks et al. 1994a), and the *bloomless2* mutant, with less epicuticular wax, exhibited more damage from sugarcane aphid than did wild-type sorghum (Harris-Shultz et al. 2020). Introducing apple wax biosynthesis genes *MdWRI4* and *MdKCS2* to Arabidopsis increased wax accumulation, and consequently improved drought and salt resistance (Lian et al. 2021; Zhang et al. 2020). The glaucous wheat was also more tolerant to drought compared to the non-glaucous one (Guo et al. 2016). Together, the accumulation of epicuticular wax protects plants from biotic and abiotic stresses, including periodic of drying and drought (Xue et al. 2017).

Epicuticular waxes can form crystals or amorphous layers, and are classified into several groups such as thin film, layers and crusts, crystalloids, or granules, platelet, rodlets, tubules, and threads (Barthlott et al. 1998). Filaments, terete in cross-section and elongated flattened ribbons are several other additional crystalloid morphologies (Jeffree 2006). Various epicuticular wax crystal shapes usually have one predominating wax chemical composition (Koch and Barthlott 2006; Jeffree 2006), such as hexacosanol and triacontanal in the platelet wax of *Pisum sativum* and *Nepenthes alata* (Macey and Barber 1970; Riedel et al. 2003), nonacaosan-10-ol in tubule wax of *Picea pungens* (Jetter and Riederer 1994), and triterpenoid β-amyrin in thread wax of *Macaranga tanarius* (Markstadter et al. 2000). Epicuticular wax morphology may be primarily influenced by its physicochemical properties but not by the properties of its underlying cuticular membrane because several crystal structures, such as tubular wax of *Picea sitchensis* and platelet wax of *P. sativum,* were reconstituted *in vitro* to their original structures (Jeffree et al. 1975). However, not all epicuticular wax crystals are able to be successfully recrystallized as for example tube wax of *Agathis australis* and *Aquilegia alpine*.

To date, several hypotheses have been proposed for the secretion of epicuticular wax: 1) the movement through cuticular pores, transcuticular canals or channels observed in various epidermal leaf tissues (Miller 1985), 2) the self-assembly process due to the ability to reconstitute the tubular crystal wax *in vitro* (Jetter and Riederer 1994), 3) the simple diffusion of wax precursors through cuticle, and 4) the transport to the epidermal surface through the cell wall and cuticle with the help of protein, lipid or carbohydrate carriers (Mcwhorter and Paul 1989; Post-Beittenmiller 1996). An attempt to recrystallize the filament wax in johnsongrass (*Sorghum halepense*) could not succeed, while the platelet wax could (Mcwhorter and Paul 1989). This finding suggests

that the platelet wax precursor may have diffused to the surface, but it also raises the possibility of a distinct secretion system for filament wax. A previous study on sorghum showed the involvement of cork cells for the secretion of filament epicuticular wax (Jenks et al. 1994b). This group also pointed out that the osmiophilic layer within the apical cork cell-wall papillae may be the secretion site for epicuticular wax, and that the wall swellings surrounding the base of papillae could be the favored route for epicuticular wax precursors. How the wax components move through cuticle cell wall and whether they are modified within the specialized cell wall layer above the cork cells remains unclear.

The epicuticular wax secretion, particularly in the leaf sheath, pseudopetiole and midrib, is highly abundant in TOM plants. Epicuticular wax accumulation has been suggested to contribute to the TOM plant resilience (Chen et al. submitted). Therefore, we aimed to analyze how and where TOM epicuticular wax is synthesized and secreted using complementary microscopy techniques, and a metabolomics analysis to find out its composition. In this study, we show that TOM secretes a uniform platelet wax together with a filament wax from specialized cork cells. The filament wax is composed of essentially C28:0 free fatty acids, on the other hand the platelet wax is predominantly composed of fatty alcohols.

MATERIALS AND METHODS

Plant materials and growth conditions

TOM Der-Wen cultivar plants were grown at a walk-in growth facility under 14 h light/10 h dark with light intensity 250 μmol m^{-2} s^{-1} and 28 °C day/25 °C night at Academia Sinica, Taiwan. Some plants were also grown in the experimental field of Academia Sinica campus under natural light conditions. The leaf blade and leaf sheath samples used for morphology study were collected from plants grown in both conditions. For the samples used for wax load analysis, the leaf blade, pseudopetiole, midrib, and leaf sheath were specifically taken from the third and fourth leaves down from the newly developed one. For the analysis of filament wax, the white powder from the leaf sheath was collected by using a brush from plants grown in the walk-in growth facility.

Histological staining

Semi-thin 1-µm cross-sections from transmission electron microscopy (TEM)-prepared samples were stained with 1 % toluidine blue in 1 % sodium borate for 30 s and rinsed with distilled water, then further observed under a Zeiss AxioImager Z1 microscope.

The leaf blade and leaf sheath were excised and cleared in a 1: 1 solution of glacial acetic acid and 30 % hydrogen peroxide for 48 h at 60 °C. Samples were then dehydrated in ethanol series and stained with Safranin-O and Fast Green (Motomura et al. 2006). Samples were imaged by using a Zeiss AxioImager Z1 microscope.

For the autofluorescence experiment, cross-section samples of leaf blade and leaf sheath were prepared manually, placed on a glass slide, and observed under a Zeiss AxioImager Z1 microscope. To observe the cell wall autofluorescence, samples were excited at 353 nm and emissions were collected at 465 nm; for chlorophyll autofluorescence, samples were excited at 575 nm to 625 nm, and emissions were collected at 660 and 710 nm (Donaldson 2020).

For lipid staining, the ClearSee method was followed (Ursache et al. 2018). Leaf blade and leaf sheath samples were excised and fixed under vacuum with 4 % paraformaldehyde in 1x phosphate buffered saline (PBS) buffer for 1-2 h. The fixed tissues were rinsed twice with 1x PBS buffer for 1 min. Samples were then cleared in ClearSee solution (xylitol [10 %], sodium deoxycholate [15 %], and urea [25 %]) for 6 days, and the solution was changed every other day. Double staining using 0.1 % Calcofluor White for cell wall staining and 0.05 % Nile Red for lipid staining was prepared in ClearSee solution. Samples were stained with this double staining solution overnight with gentle agitation and rinsed with ClearSee solution twice for 30 min and 1 h. For visualization, samples were placed in glass slides and imaged under a Zeiss LSM 510 META confocal laser scanning microscopy. Nile Red staining was imaged at 561 nm excitation and detected at 600-650 nm, and Calcofluor White at 405 nm/425-475 nm.

Scanning electron microscope (SEM) observation

Cryo-SEM observation was performed using FEI Quanta 200 with a cryo system, Quorum PP2000TR FEI. Excised leaf blades and leaf sheaths were frozen in liquid nitrogen and placed into the preparation chamber and examined at -160 °C for 5 min. After the temperature reached -85 °C, samples were sublimed for 15 min, and

coated with platinum at -130 °C, then transferred to the cryo stage inside the SEM chamber and imaged at -180 °C to -190 °C with 20 kV (Chang et al. 2019).

Transmission electron microscopy (TEM) observation

TEM samples were prepared as described (Chang et al. 2019) with some modification. Leaf blades and leaf sheaths were excised to a 1 cm x 1 cm rectangle size and fixed in 2.5 % glutaraldehyde and 0.05 M cacodylate buffer at room temperature for 4 h. After three rinses with 0.1 M sodium phosphate buffer (pH 7.0), the samples were post-fixed in 1 % osmium tetroxide in the same buffer for 4 h and rinsed three times with the previous buffer. Samples were dehydrated in ethanol series and transferred to prophylene oxide, then embedded in Spurr's resin. The semi-thin cross-sections were prepared in 1-µm sections by using the ultramicrotome Leica Reichert Ultracut S and further stained with toluidine blue. The ultrathin sections of 70-90 nm were prepared with the ultramicrotome, then stained with uranyl acetate and lead citrate. Sample images were taken by using the FEI Tecnai G2 Spirit at 80 kV. TrakEM2 was used to develop the montage images (Cardona et al. 2012).

Wax component analysis

Cuticular wax analyses of various organs of TOM plants involved using gas chromatography–mass spectrometry (GC-MS) (Fernandez-Moreno et al. 2016; Busta et al. 2021). Total wax abundance was calculated from measured surface areas of tissue that had been excised from various organs: leaf blade, leaf sheath, pseudopetiole and midrib. Wax was extracted by immersing the sample in chloroform twice for 30 s and spiked with an internal standard of tetracosane or docosane (10 µg), then chloroform was evaporated under N_2 stream. The residue was derivatized with 150 µl *N,O*-bis(trimethylsilyl)-trifluoro-acetamide with 1 % trimethylchlorosilane at 85 °C for 1 h. Samples were dissolved in 400 µl hexane and subjected to GC analysis by using Agilent 7890 with a DB-5MS column (30 m × 0.250 mm × 0.25 µm), with helium as the carrier gas (1.2 mL min^{-1}). The oven program condition was initial temperature for 0 min at 65 °C, followed by 20 °C min^{-1} to 220 °C, 3 min at 220 °C, 3 °C min^{-1} to 300 °C, 0 min at 300 °C, 5 °C min^{-1} to 310 °C, 35 min at 310 °C. Analytes were detected by using the Agilent 5975C mass spectrometric detector (70 eV, m/z 50-850). Eluted

compounds after 10 min were analyzed.

Additional standards, C_{28} alcohol (Sigma), C_{28} and C_{30} fatty acids (Sigma), and the C_{21}-C_{40} alkane mix (Sigma), were also used to confirm the reproducibility of compound retentions. For total wax abundance, the total sample weight was obtained by quantifying each peak area compared to the internal standard and divided by the area of tissue samples. Except for the brushed wax, the wax abundance was divided by milligrams dry weight. Typically, a <20 cm^2 area was used for analysis of leaf blades and leaf sheaths and <10 cm^2 for pseudopetioles and midribs. The surface area of leaf blades was calculated as 2 x length x width. The surface area of leaf sheaths was calculated as л x diameter x height, and the pseudopetioles and midribs were calculated as (л x diameter x height)/2 + (length x width).

RESULTS

The phenotype of Taiwan oil millet (TOM) plant

The TOM plant can bear several tillers or inflorescences (Fig. 1a), and reach about 80-180 cm height in the field until heading stage (Fig. S1a). The leaf consists of a sheath that covers the culm or stem and overlaps one another at the base (Fig. 1b), a blade consisting of a flat and elongated lamina with parallel veins, and a pseudopetiole, the organ junction between leaf sheath and blade. In one tiller, all the leaves are connected to leaf sheath with a pseudopetiole (Fig. S1b). The abaxial surface of the leaf sheath and both abaxial and adaxial sides of the pseudopetiole are conspicuously coated with white powdery epicuticular wax (Fig. S1c-e), but it is less abundant on the midrib. In particular, the shallow groove on the adaxial surface of pseudopetiole helps to retain the accumulated white powdery wax. At the joint between leaf sheath and pseudopetiole lies two specific structures–ligule and auricle (Fig. S1e).

The platelet wax present more ubiquitous than the short filament wax in TOM leaf blade

We initially identified the different cell types in the cross-section of leaf blade using Toluidine blue staining. This revealed a single-layer epidermis in both adaxial and abaxial surfaces, and variable sizes of irregular

shaped mesophyll cells that radially encircled the bundle sheath, and also closer vein spacing as a characteristic of a C_4 leaf (Fig. 2a). The first-order or largest vascular bundle appeared less frequent, while the second- and third-order were alternatively organized. Bulliform-like cells existed on the adaxial epidermis as ballooned cells between epidermal cells flanking the vascular bundles. Autofluorescence imaging showed an enrichment of chloroplasts in the mesophyll cells surrounding the bundle sheath, as indicated by the bright red fluorescence (Fig. 2b). A recent study in *Arabidopsis* showed that the number of chloroplasts in pavement cells was only one-tenth of that of the mesophyll cells and was present in a sparse arrangement (Barton et al. 2016), which coincided with our observations.

To identify the distinct cell type present in the adaxial surface of leaf blade, Safranin O and Fast Green staining were used. Fig. 2c illustrates the arrangement of parallel long cells with corrugated cell wall above the vascular bundle (costal) and between the vascular bundle (intercostal). Above the larger vascular bundle, silica cells and cork cells were alternately arranged in a single horizontal row, together with prickle hair that appeared less frequently. The silica cells stained greyish white and were dumbbell-shaped, whereas the cork cells stained as red, appeared as narrow-crenated rectangles, and in some cases, appeared extended or fused into longer forms. It has been suggested that in oat, the short cells generally appeared as narrow crenated rectangle-like cork cells could become pairs of silica-cork cells, prickle hairs or micro hairs, and stomata (Kaufman et al. 1970b). These cork cells as well as the crenated short cells were lipid-rich, as they are strongly stained with Nile Red (Fig. S2a-c). Nile Red stains suberin and lipid rich cells, whereas Calcofluor White stains cell walls containing chitin, cellulose, or other beta-1,4-linked carbohydrates (Ursache et al. 2018). Likewise, these structures were also observed in SEM images (Fig. 2d, e). The platelet wax covered most of the surface of both costal and intercostal long cells, whereas the filament wax was short and detected overlapping with the cork cells (Fig. 2d, e).

The abaxial surface of the leaf blade also consisted of a parallel line of long cells, in which the intercostal long cells were slightly broader than the costal ones (Fig. S3a, b). Two parallel lines of stomata were situated alternately with long cells in this intercostal area, forming a ladder-like structure. These long cells were covered with more obvious rounded structures of papillae, and one long cell usually harbored four to six papillae.

Discerning the silica and cork cells in this abaxial leaf blade was difficult because they were buried among the papillae of long cells covered with platelet wax (Fig. S3a). Nevertheless, there were certain areas in these costal cells covered with larger platelet waxes (Fig. S3c, d). Nile Red and Calcofluor White staining also showed that the silica and cork cells were alternately arranged in a single row above the major vein and were dumbbell-shaped, but the silica cells usually had a more extended or fused dumbbell shape appearance (Fig. S2d-f). Overall, our data indicated that platelet wax was predominantly secreted by the adaxial and abaxial epidermal cells of the leaf blade, and only short filament wax present in the adaxial surface, overlaying with the cork cell. For the midrib (Fig. S4a-c) and pseudopetiole (Fig. S4d-e), longer wax filaments were secreted more abundantly than platelet wax, but both lacked the dumbbell-shaped silica cells.

Filament wax abundantly secreted in the TOM leaf sheath

Because of copious secretion of white powder in TOM leaf sheath, we examined its anatomy using Toluidine blue staining. This revealed that the epidermal cells of the abaxial side had relatively thicker cell walls than the adaxial side (Fig. 3a). Major and minor vascular bundles were arranged alternately and developed only at the abaxial side. Chloroplasts were enriched in the mesophyll cells of the abaxial outer side, surrounding the bundle sheath of the leaf sheath, but were not detected towards the inner adaxial surface (Fig. 3b). This result illustrates the importance of cellular architecture for optimizing photosynthesis and gas exchange.

We characterized the morphological structure on the abaxial surface of leaf sheath, different cell types were easily distinguished by Safranin O and Fast Green staining. Contrary to the leaf blade, the pair of silica and cork cells were not limited to the costal area, but were also present in the intercostal long cell rows (Fig. 3c). In the costal area, the silica and cork cells frequently appeared independently with an extended form or a fused dumbbell-like shape. However, in the intercostal area, the cork cell appeared as crenated rectangle short cells, while silica cell took shape of dumbbell or butterfly, and they both co-existed as a pair. We also noticed the presence of solitary cork cells, but not silica cells. This supports the previous observation that silica cell arise from the division of cork cell (Kaufman et al. 1970a). These crenated short cork cells were also markedly stained by Nile Red, suggesting a high lipid content (Fig. S2g-i).

To determine the wax type present in the leaf sheath, we used SEM. This showed that the filament wax in leaf sheath were extensive, longer, extruded more prolifically than in the leaf blade. The filament clusters specifically protruded out from the specific site of the leaf sheath, aligned to the width of one cell (Fig. 3d). Platelet wax was also present on this abaxial leaf sheath, but the conspicuous white powder mainly consisted of the filament wax. In contrast, both platelet and filament waxes were absent from the adaxial surface of the leaf sheath and only covered by smooth film of epicuticular wax devoid of crystals (Fig. 3e). Only few stomata were sparsely distributed in these parallel long cells of adaxial leaf sheath. Table 1 summarizes the detailed comparison of the presence of specific cell types on both the adaxial and abaxial surfaces of both leaf blade and leaf sheath.

Filament wax secretion by specific cork cells in the leaf sheath and leaf blade

To identify the cells responsible for epicuticular filament wax secretion, we brushed off the existing waxes, and the newly synthesized filament wax emerged from the cork cell surface, as observed with SEM (Figs. 4a, S5a-c). The cork cell appeared adjacent to the silica cell with a butterfly or dumbbell shape and a concave surface. The filament wax protruded out as a single or double linear array of pores at the basal and distal sides of the cork cell, or more pores at its periphery, encircling the cork cell upon expansion with varied length. The filament wax were freeze-fractured under the cryo-SEM observation, revealing a hollow structure inside (Fig. 4b), consistent with previous observation of sorghum filament wax (Jenks et al. 1994b).

The confocal cross-section image of the leaf sheath stained with Nile Red (Fig. 4c) indicated lipid enrichment specifically in the tangential surface of the cork cell wall, but not in the other neighboring epidermal cells, where Nile Red only slightly stained the surface (i.e. the cuticle). Within this cork cell wall, we observed a conical shape papillae protrusion toward the aerial surface, which was strongly stained by Nile Red, suggesting an association with polar lipid, i.e. free fatty acids. The cross-section of leaf sheath ultrastructure image revealed that the cork cell had a thinner cell wall as compared with the neighboring abaxial epidermal cells (Fig. 4d). The tangential surface of the cork cell had two layers of cell wall, in which the inner primary cell wall directly next to the plasma membrane was thinner than the second outer layer with darker staining. The undulated surface of

281 cork cell papillae is likely the site for conical protrusion of filament wax, which coincided with a markedly Nile
282 Red-stained convex papillae protrusion. The cork cells usually have apparent dark dense cytoplasm, which
283 suggests that it is highly metabolically active (Fig. 4d). This was also seen in longitudinal and paradermal
284 sections (Fig. S6a, b). These silica and cork cells were frequently occurred in pairs, and the dumbbell-shaped
285 silica cells clearly accumulated rod-like silica bodies, which were shattered in certain parts due to sample
286 preparation difficulties (Fig. S6a, b). Dark-stained small spheres (Fig. 4e) were observed along the first inner
287 layer of cork cell walls, including below the papillae protrusion tip (Fig. S6c). The uppermost, darkest layer
288 above the cork cell wall showed different characteristics from the corresponding position of cork cells in Fig. 4e
289 as visualized by TEM. However, this layer did not stain by Nile Red (Fig. 4c), suggesting that it is not lipid-rich
290 and possibly overlays of the adjacent silica cell as previously described in *Lolium temulentum* epidermal
291 internode (Lawton 1980). Silica in the lumen of silica and bulliform cells were reported as rod-shaped, whereas
292 in the trichomes and long epidermal cell wall matrix were spherical masses form (Kaufman et al. 1985).
293 Since short filament waxes were still detected in the leaf blade, we also examined the ultrastructure of its
294 cork cell. Consistent to the leaf sheath observation, the TEM transverse section of cork cell leaf blade (Fig. S7a)
295 revealed two layers in the tangential cell wall: a lighter inner cell wall, and a thicker and darker outer cell wall.
296 Additionally, there was an outermost epicuticular wax film that also covered the neighboring epidermal cells.
297 Compared to the leaf sheath cork cell, the unstained darkest layer (Fig. 4d, e) and the papillae were absent in this
298 leaf blade cork cell. In case of papillae absence, it is possible that the filament secretion in a leaf blade was not a
299 continuous process, since only short filament wax was detected, or there was less production of C28:0 fatty acid.
300 The silica cell of leaf blade also appeared in the middle, overlying vascular bundle (Fig. S7b), containing rod-
301 like silica bodies.
302 TEM image of TOM leaf sheath abaxial epidermal cells also revealed peculiar structures of cytoplasmic
303 protrusion. These protrusions were not restricted to the corners of one cell toward cell surface as seen in
304 transverse section (Fig. S8a, b). Instead, several exvaginations also appeared along one epidermal cell toward
305 the abaxial surface in longitudinal section (Fig. S8c). Osmiophilic globules or vesicles were often associated
306 with this cytoplasmic constriction. The closest tip distance of this cytoplasmic constriction reaching to the

epidermal surface was approximately 0.4 μm based on our various observations. The physiological role of these cytoplasmic constrictions is unclear: whether it is merely the result of interdigitation between adjacent corrugated epidermal cell wall, or to allow the expansion of leaf sheath epidermal cells during growth, or related to a secretion function including assisting the secretion of neighboring cork cells.

Epicuticular wax composition analysis by GC

We also examined the composition of TOM wax mixture in various organs: leaf blade, midrib, pseudopetiole and leaf sheath as well as the brushed wax collected from both the leaf sheath and pseudopetiole. GC-MS analysis showed that the leaf blade wax mixture was primarily composed of C28:0 primary alcohol (61 % of the total) and C_{28} aldehyde (12 %; Fig. 5a). The amount of the predominant alcohol compound class, which also contained C_{32} (4.75 %) and C_{26} (1.25 %), was 13.75 μg cm^{-2} in leaf blade epicuticular wax (Fig. 5a, Table 2). Other compounds present in the wax mixture in limited amount were C_{21} methyl alkyl-resorcinol (3.7 %) and C_{28} fatty acid (3 %). Of note, the major chain length detected in the leaf blade epicuticular wax mixture was 28–carbons, in alcohols, aldehydes and fatty acids.

The midrib wax mixture analysis indicated fatty acids as the primary constituents (83 %), with a load of 48.74 μg cm^{-2} (Table 2, Fig. 5b). The C_{28} alcohol was the second most abundant compound class, followed by aldehyde, alkane and alkylresorcinol in trace amounts. The epicuticular wax of leaf sheath and pseudopetiole were remarkably constituted by nearly exclusively fatty acids with 98 % of the total (Fig. 5c, d) that comprised ~90 % C_{28}, followed by C_{26} and C_{30}. The main composition of leaf sheath wax was even-numbered fatty acids ranging from C_{22}-C_{30}, but odd-numbered fatty acids (C_{27} and C_{29}) were also present in minor quantities. Notably, the wax compositions of leaf sheath, midrib, and pseudopetiole were highly dominated by C_{28} fatty acid.

The main components of the brushed wax were fatty acids (96 %; Fig. 5e) with the predominant C_{28}, while no alcohol compound classes were detected. Finally, when comparing the wax production of these various organs, the pseudopetiole had the highest amount, followed by leaf sheath, midrib, and leaf blade (Fig. 5f). The wax load for brushed wax was 353 μg mg DW^{-1}. The aforementioned data suggested that C_{28} fatty acids predominated the wax composition of TOM leaf sheath, pseudopetiole, midrib and brushed wax, with the

filament-shaped wax as the primary shape of epicuticular wax. Conversely, the leaf blade contained C_{28} alcohol as major wax and platelet wax as the major epicuticular wax crystals. The midrib epicuticular wax mixture still contained very little amounts of C_{28} alcohol, which could be a result of some traces of leaf blade during sample preparation. This is in contrast to leaf sheath and pseudopetiole, where C_{28} alcohol was barely detected, and further supports that platelet wax mainly consisted in C_{28} alcohol.

DISCUSSION

Our study of TOM morphology and wax composition revealed that 1) different kinds of wax crystal were present on the different organs, 2) the filament wax was abundantly secreted by the cork cells present in the abaxial epidermal surface of leaf sheath, and 3) certain compound classes specifically corresponded to the distinct type of epicuticular wax crystals, particularly filament wax that were remarkably constituted by 90 % C_{28} free fatty acid (octacosanoic acid or montanic acid), while it represented only 77 % in sorghum (Jenks et al. 2000).

Two kinds of epicuticular wax crystal differentially dominated in particular organs

In this study, we identified two kinds of epicuticular wax crystals: platelet and filament types present in TOM leaf blade, leaf sheath, pseudopetiole and midrib. Platelet wax was evenly distributed in the epidermal cells of these various organs, but filament wax was restricted to the cork cells (Figs. 2d-e, S3a-d, 3d-e). Although filament wax was secreted by the leaf blade cork cells, it was not to the same extent as in the leaf sheath. Not only the leaf sheath, but pseudopetiole and midrib of TOM also have conspicuous white powder (Fig. S1c-e), and our data verified that they are rich in filament wax (Fig. S4a-e). However, the absence of cork cells in the adaxial leaf sheath results in the clearance from any crystal filament wax. Similar observations were also noted in sorghum, with no wax crystal on leaf sheath adaxial surfaces (Jenks et al. 2000), which suggests that external environment may modify physical form of wax and epicuticular wax crystal present on the aerial surface exposed to ambient air acts as a protection mechanism.

Filament wax projection through the papillae of cork cells

Here, we have shown that the filament wax, including newly synthesized one, protrudes out from the leaf sheath cork cell adjacent to the dumbbell-shaped silica cells (Figs. 4a, S5a-c). This supports previous studies in *Sorghum halepense* and *S. bicolor* (Mcwhorter and Paul 1989; Jenks et al. 1994b), which also found that filament wax is synthesized by cork cells instead of silica cells. TOM filament wax is a hollow structure with the diameter of 1-1.6 μm (Fig. 4b), which is similar to the 1.1 μm diameter reported in sorghum (Jenks et al. 1994b).

The cork cell ultrastructural image revealed two layers of cork cell wall: a thinner inner layer and a thicker outer layer highly stained by Nile Red (Fig. 4c, d), suggesting that they are lipophilic. The conical papillae in the apical walls of epidermal cork cells in sorghum may be the site for protrusion of circular array of pores (Jenks et al. 1994b). TOM filament wax emerged from cork cells, and one epidermal cork cell indeed could have several papillae protrusion, as visualized by SEM, TEM and Nile Red staining (Fig. 4a-d). Therefore, our data also support that the papillae at the tip of cork cells could be the point of origin for the filament wax protrusion to the aerial plant surface. Although the wax secretion to the surface via pores is not a favorable hypothesis as in the case for platelet and tubular wax, the fact that the Nile Red stained specifically these papillae sites in a cork cell suggests they could be a path for filament wax extrusion to the plant surface. The average width of papilla in the cork surface was 1.04 ± 0.09 μm, which corresponds well to the above-mentioned width of filament wax in aerial surface. The cork cell as an idioblast arises from asymmetric division of initial protoderm cells or costal short cells and continuously divides and differentiates, resulting in a pair of cork-silica cells, as studied in *Avena* or other grasses (Kaufman et al. 1971; Kaufman et al. 1970b). The undulated papillae structure was absent at the external periclinal cork cell wall of *L. temulentum* and *A. sativa* (Kaufman et al. 1970a; Lawton 1980), which could possibly indicate that these papillae are present exclusively in sorghum and TOM for the secretion of epicuticular filament wax. The independent cork cell without silica cell we observed could also likely be in their early development and not yet differentiated, and still secreted filament wax.

Similar to TOM, a dense cytoplasm characteristic of cork cell (Figs. 5d, S6a-b) also exist in the other species e.g. *L. temulentum, A. sativa, S. halepense* and *S. bicolor* (Mcwhorter and Paul 1989; Jenks et al. 1994b;

385 Kaufman et al. 1970a; Lawton 1980). TOM cork cells with dense cytoplasm may reflect extraordinarily high
386 metabolism to sustain intense production of very-long chain fatty acids in the endoplasmic reticulum. Other cell
387 type with this characteristic include colleters, which are secretory structures of epidermal cells present at the
388 base of stipule of genus *Simira* family of Rubiaceae containing protein and carbohydrates possibly involved in
389 defense mechanisms (Klein et al. 2004). The capsaicinoid-secreting cells in placentae epidermis of red pepper
390 (*Capsicum annuum*), which contribute to the level of spiciness, also had dense cytoplasm (Zamski et al. 1987).
391 Thus, this dark dense cytoplasm may be related to the secretory function of these cells.
392 Furthermore, spherical structures with approximately 60-nm diameter or less were observed along the
393 inner cork cell wall spreading below the papillae (Figs. 4e, S6c), that could be the filament wax precursors or
394 the precursors for the outer lipophilic layer of cork cell. More apparent and larger spherical structures were also
395 observed in another study on oil millet accessions that were wax-rich or wax-less (data not shown). Such
396 spherical structures associated with epicuticular wax secretion have not been reported. Our findings also support
397 previous hypotheses (Smith et al. 1978; Mcwhorter and Paul 1989) whereby the wax precursors surround the
398 cork cell wall and are transported out through the cuticle by lipo- or glycoprotein, which remains to be
399 identified.
400
401 **Distinct epicuticular wax crystal might correspond to distinct wax metabolites**
402 It has been proposed that wax crystal structure can be determined by its dominating compound (Barthlott et al.
403 1998; Jeffree 2006). Although we are not able to exclude the presence of only single wax crystal in these
404 different TOM organs, we could relate the presence of specific compound to the dominance of certain wax
405 crystal. Platelet wax as the majority of wax crystal present on the leaf blade is associated with a high
406 concentration of primary alcohols. These primary alcohols of platelet wax have also been observed in wheat flag
407 leaf blade, rice leaf blade and leaf sheath, and adaxial leaf surface of *L. perenne* (Wang et al. 2015a; Mao et al.
408 2012; Racovita et al. 2016; Ringelmann et al. 2009). Tubule-shape wax present in the wheat peduncle comprised
409 mainly β-diketones (Wang et al. 2015a; Racovita et al. 2016). Previous study of sorghum indicated that free fatty
410 acids predominated the composition of its leaf sheath cuticular waxes, at 96 %, with C_{28} and C_{30} accounting for

411 76 % and 20 % (Jenks et al. 2000). This result also consistent with TOM leaf composition accounted for 98 % of
412 the total, and intriguingly contributed by the singular dominant of C_{28} fatty acid representing 90 %. The second
413 highest compound in TOM is C_{26} fatty acid (6.5 %), while in sorghum it is C_{30}. Our results support that free fatty
414 acid, and C_{28} in particular, is the main constituent for filament wax in these two plants. In sorghum, the
415 epicuticular wax analyses suggested that C_{28} and C_{30} fatty acids were the constituents of both filament and
416 platelet waxes because in the bloomless *bm11* mutant, which has only the platelet wax but no filaments, similar
417 proportions for these two dominant fatty acids were found (Jenks et al. 2000). In contrast to their results, our
418 data clearly demonstrate that filament wax predominantly exists in leaf sheath and primarily composed of C_{28}
419 fatty acids (Fig. 5c), whereas platelet wax that is enriched in leaf blade consists of almost two-thirds C_{28} alcohol
420 (Fig. 5a) suggesting their unique chemical composition for distinct wax crystal. Additionally, filament wax
421 accounts for most epicuticular wax crystals in midrib, pseudopetiole and brushed wax yielded the similar
422 percentage fatty acid composition as in leaf sheath (Fig. 5b-e) suggesting that the filament wax indeed
423 comprised of mainly fatty acid. The wax load of TOM leaf sheath was slightly higher compared to sorghum
424 (Jenks et al. 2000), but TOM pseudopetiole had the highest wax load compared to other organs.
425 Of note, the chain length distribution for both platelet and filament wax present in leaf blade and leaf
426 sheath is predominantly C_{28} carbon in length. This finding indicates that the substrate preference of the ketoacyl-
427 CoA synthase favors C26:0 acyl-CoA, similar to that of wheat (Racovita et al. 2016). The platelet wax present in
428 the TOM leaf blade could result from further conversion to the very long chain primary alcohol by the *CER4* or
429 a homologue of the wheat *TaFAR5* gene (Wang et al. 2015b), and to the aldehyde possibly involving an
430 aldehyde-forming fatty acyl-CoA reductase (Vioque and Kolattukudy 1997), whereas the free fatty acid could be
431 formed by thioesterase (Batsale et al. 2021).
432 Collectively, our data show that TOM plants have more numerous cork cells not limited to costal area but
433 also intercostal such as in the abaxial surface of leaf sheath, and therefore contribute to the vastly dense
434 secretion of filament wax. Our study revealed that TOM plant produced abundant epicuticular filament wax
435 specifically synthesized by cork cells through papillae extrusion. Further studies will be required to decipher
436 whether the spheres in the inner wall of cork cell are indeed the precursors of filament wax to be delivered to the

plant surface. Given that highly abundant production of filament wax in TOM made it more resilience against harsh environment including both biotic and abiotic stress, it is important to conserve this TOM plant and to explore its full potential for crop and plant breeding purpose.

AUTHOR CONTRIBUTIONS

YICH conceived and designed the study. MA, YYL, SAF, HPW, CCW and WNJ performed the experiments. TJR and FD contributed to the metabolomics analysis experiment. MA analyzed the data, and MA, YICH, TJR and FD wrote the manuscript. YICH acquired the funding and supervised the study. All authors approved the submitted manuscript.

ACKNOWLEDGEMENTS

This work was financially supported by the Innovative Translational Agricultural Research (ITAR) Taiwan (2018PRE050, AS-108-ITAR-L05, AS-109-ITAR-L05, AS-110-ITAR-L01). We thank Ms. Lie-Hong Wu for greenhouse maintenance; Ms. Mei-Jane Fang and Mr. Ji-Ying Huang for technical assistance in the microscope facility (Live-Cell-Imaging Core Lab of IPMB, Academia Sinica): Chia-Me Hsu, Yi-Chia Chou for TEM and SEM assistance (Electron Microscope of IPMB, Academia Sinica); Yu-Ching Wu (Small Molecules Metabolomics Core Lab of IPMB, Academia Sinica) for GC-MS facility maintenance; and Ms. Laura Smales for English editing.

DATA AVAILABILITY STATEMENT

All relevant data are presented in this paper.

DECLARATIONS

CONFLICT OF INTEREST

The authors declare no conflict of interest or any other kind.

REFERENCES

Barthlott W, Neinhuis C, Cutler D, Ditsch F, Meusel I, Theisen I, Wilhelmi H (1998) Classification and terminology of plant epicuticular waxes. Bot J Linn Soc 126 (3):237-260. doi:10.1111/j.1095-8339.1998.tb02529.x

Barton KA, Schattat MH, Jakob T, Hause G, Wilhelm C, McKenna JF, Mathe C, Runions J, Van Damme D, Mathur J (2016) Epidermal Pavement Cells of Arabidopsis Have Chloroplasts. Plant Physiol 171 (2):723-726. doi:10.1104/pp.16.00608

Batsale M, Bahammou D, Fouillen L, Mongrand S, Joubes JM, Domergue F (2021) Biosynthesis and Functions of Very-Long-Chain Fatty Acids in the Responses of Plants to Abiotic and Biotic Stresses. Cells-Basel 10 (6). doi:10.3390/cells10061284

Busta L, Schmitz E, Kosma DK, Schnable JC, Cahoon EB (2021) A co-opted steroid synthesis gene, maintained in sorghum but not maize, is associated with a divergence in leaf wax chemistry. Proc Natl Acad Sci U S A 118 (12). doi:10.1073/pnas.2022982118

Cardona A, Saalfeld S, Schindelin J, Arganda-Carreras I, Preibisch S, Longair M, Tomancak P, Hartenstein V, Douglas RJ (2012) TrakEM2 Software for Neural Circuit Reconstruction. Plos One 7 (6). doi:10.1371/journal.pone.0038011

Chang CL, Serapion JC, Hung HH, Lin YC, Tsai YC, Jane WN, Chang MC, Lai MH, Hsing YC (2019) Studies of a rice sterile mutant sstl from the TRIM collection. Bot Stud 60 (1):12. doi:10.1186/s40529-019-0260-3

Donaldson L (2020) Autofluorescence in Plants. Molecules 25 (10). doi:10.3390/molecules25102393

Fernandez-Moreno JP, Malitsky S, Lashbrooke J, Biswal AK, Racovita RC, Mellerowicz EJ, Jetter R, Orzaez D, Aharoni A, Granell A (2016) An efficient method for medium throughput screening of cuticular wax composition in different plant species. Metabolomics 12 (4). doi:10.1007/s11306-016-0982-0

Grass Phylogeny Working G, II (2012) New grass phylogeny resolves deep evolutionary relationships and discovers C4 origins. New Phytol 193 (2):304-312. doi:10.1111/j.1469-8137.2011.03972.x

Guo J, Xu W, Yu XC, Shen H, Li HS, Cheng DG, Liu AF, Liu JJ, Liu C, Zhao SJ, Song JM (2016) Cuticular Wax Accumulation Is Associated with Drought Tolerance in Wheat Near-Isogenic Lines. Frontiers in Plant Science 7. doi:10.3389/fpls.2016.01809

Harris-Shultz K, Punnuri S, Knoll JE, Ni X, Wang H (2020) The sorghum epicuticular wax locus Bloomless2 reduces plant damage in P898012 caused by the sugarcane aphid. Agrosyst Geosci Environ 3:e20008

Henry A (1904) *Spodiopogon formosanus*, Rendle. The Journal of the Linnean Society Botany 36:351-352

500 Jeffree CE (2006) The fine structure of the plant cuticle. In: Riederer M, Muller C (eds)
501 Biology of the Plant Cuticle. Blackwell, Oxford, pp 11-115
502 Jeffree CE, Baker EA, Holloway PJ (1975) Ultrastructure and Recrystallization of Plant
503 Epicuticular Waxes. New Phytologist 75 (3):539-+. doi:10.1111/j.1469-
504 8137.1975.tb01417.x
505 Jenks MA, Joly RJ, Peters PJ, Rich PJ, Axtell JD, Ashworth EN (1994a) Chemically-Induced
506 Cuticle Mutation Affecting Epidermal Conductance to Water-Vapor and Disease
507 Susceptibility in Sorghum-Bicolor (L) Moench. Plant Physiology 105 (4):1239-1245.
508 doi:10.1104/pp.105.4.1239
509 Jenks MA, Rich PJ, Ashworth EN (1994b) Involvement of Cork Cells in the Secretion of
510 Epicuticular Wax Filaments on Sorghum-Bicolor (L) Moench. Int J Plant Sci 155
511 (5):506-518. doi:10.1086/297190
512 Jenks MA, Rich PJ, Rhodes D, Ashworth EN, Axtell JD, Ding CK (2000) Leaf sheath cuticular
513 waxes on bloomless and sparse-bloom mutants of Sorghum bicolor. Phytochemistry
514 54 (6):577-584. doi:10.1016/S0031-9422(00)00153-9
515 Jetter R, Riederer M (1994) Epicuticular Crystals of Nonacosan-10-Ol - in-Vitro Reconstitution
516 and Factors Influencing Crystal Habits. Planta 195 (2):257-270
517 Kaufman PB, Dayanandan P, Franklin CI, Takeoka Y (1985) Structure and Function of Silica
518 Bodies in the Epidermal System of Grass Shoots. Ann Bot-London 55 (4):487-507.
519 doi:10.1093/oxfordjournals.aob.a086926
520 Kaufman PB, Petering LB, Smith JG (1970a) Ultrastructural Development of Cork-Silica Cell
521 Pairs in Avena Internodal Epidermis. Bot Gaz 131 (3):173-&. doi:10.1086/336529
522 Kaufman PB, Petering LB, Soni SL (1971) Ultrastructural Studies on Cellular Differentiation in
523 Internodal Epidermis of Avena Sativa. American Journal of Botany 58 (5):450-&
524 Kaufman PB, Petering LB, Yocum CS, Baic D (1970b) Ultrastructural Studies on Stomata
525 Development in Internodes of Avena-Sativa. American Journal of Botany 57 (1):33-&.
526 doi:10.2307/2440378
527 Kew RBG (2022) http://specimens.kew.org/herbarium/K000309024. Accessed July 2022
528 Klein DE, Gomes VM, Da Silva-Net SJ, Da Cunha M (2004) The structure of colleters in several
529 species of Simira (Rubiaceae). Ann Bot-London 94 (5):733-740.
530 doi:10.1093/aob/mch198
531 Koch K, Barthlott W (2006) Plant epicuticular waxes: Chemistry, form, self-assembly and
532 function. Nat Prod Commun 1 (11):1067-1072
533 Koch K, Neinhuis C, Ensikat HJ, Barthlott W (2004) Self assembly of epicuticular waxes on
534 living plant surfaces imaged by atomic force microscopy (AFM). J Exp Bot 55
535 (397):711-718. doi:10.1093/jxb/erh077
536 Lawton JR (1980) Observations on the Structure of Epidermal-Cells, Particularly the Cork and
537 Silica Cells, from the Flowering Stem Internode of Lolium-Temulentum L (Gramineae).

538 Bot J Linn Soc 80 (2):161-177. doi:10.1111/j.1095-8339.1980.tb01663.x
539 Lian XY, Gao HN, Jiang H, Liu C, Li YY (2021) MdKCS2 increased plant drought resistance by
540 regulating wax biosynthesis. Plant Cell Reports 40 (12):2357-2368.
541 doi:10.1007/s00299-021-02776-4
542 Macey MJK, Barber HN (1970) Chemical Genetics of Wax Formation on Leaves of Pisum-
543 Sativum. Phytochemistry 9 (1):5-&. doi:10.1016/S0031-9422(00)86608-X
544 Mao BG, Cheng ZJ, Lei CL, Xu FH, Gao SW, Ren YL, Wang JL, Zhang X, Wang J, Wu FQ, Guo XP,
545 Liu XL, Wu CY, Wang HY, Wan JM (2012) Wax crystal-sparse leaf2, a rice homologue of
546 WAX2/GL1, is involved in synthesis of leaf cuticular wax. Planta 235 (1):39-52.
547 doi:10.1007/s00425-011-1481-1
548 Markstadter C, Federle W, Jetter R, Riederer M, Holldobler B (2000) Chemical composition of
549 the slippery epicuticular wax blooms on Macaranga (Euphorbiaceae) ant-plants.
550 Chemoecology 10 (1):33-40. doi:10.1007/s000490050005
551 Mcwhorter CG, Paul RN (1989) The Involvement of Cork-Silica Cell Pairs in the Production of
552 Wax Filaments in Johnsongrass (Sorghum-Halepense) Leaves. Weed Sci 37 (3):458-
553 470. doi:10.1017/S0043174500072222
554 Miller RH (1985) The Prevalence of Pores and Canals in Leaf Cuticular Membranes. Ann Bot-
555 London 55 (4):459-471. doi:10.1093/oxfordjournals.aob.a086924
556 Motomura H, Fujii T, Suzuki M (2006) Silica deposition in abaxial epidermis before the
557 opening of leaf blades of Pleioblastus chino (Poaceae, Bambusoideae). Ann Bot-
558 London 97 (4):513-519. doi:10.1093/aob/mcl014
559 Post-Beittenmiller D (1996) Biochemistry and Molecular Biology of Wax Production in Plants.
560 Annu Rev Plant Physiol Plant Mol Biol 47:405-430.
561 doi:10.1146/annurev.arplant.47.1.405
562 Racovita RC, Hen-Avivi S, Fernandez-Moreno JP, Granell A, Aharoni A, Jetter R (2016)
563 Composition of cuticular waxes coating flag leaf blades and peduncles of Triticum
564 aestivum cv. Bethlehem. Phytochemistry 130:182-192.
565 doi:10.1016/j.phytochem.2016.05.003
566 Riedel M, Eichner A, Jetter R (2003) Slippery surfaces of carnivorous plants: composition of
567 epicuticular wax crystals in Nepenthes alata Blanco pitchers. Planta 218 (1):87-97.
568 doi:10.1007/s00425-003-1075-7
569 Riederer M (2006) Introduction: biology of the plant cuticle. In: Riederer M, Muller C (eds)
570 Biology of the Plant Cuticle. Blackwell, Oxford, pp 1-10
571 Ringelmann A, Riedel M, Riederer M, Hildebrandt U (2009) Two sides of a leaf blade:
572 Blumeria graminis needs chemical cues in cuticular waxes of Lolium perenne for
573 germination and differentiation. Planta 230 (1):95-105. doi:10.1007/s00425-009-
574 0924-4
575 Smith LC, Pownall HJ, Gotto AM, Jr. (1978) The plasma lipoproteins: structure and

metabolism. Annu Rev Biochem 47:751-757. doi:10.1146/annurev.bi.47.070178.003535

Soreng RJ, Peterson PM, Romaschenko K, Davidse G, Teisher JK, Clark LG, Barbera P, Gillespie LJ, Zuloaga FO (2017) A worldwide phylogenetic classification of the Poaceae (Gramineae) II: An update and a comparison of two 2015 classifications. J Syst Evol 55 (4):259-290. doi:10.1111/jse.12262

Takei E Millet Culture and Indigenous Cuisine in Taiwan. In: Proceedings of the International Symposium on Chineese Food Culture, 2013. vol 13. pp 193-210. doi:10.6641/piccfc.13.2013.13.08

Ursache R, Andersen TG, Marhavy P, Geldner N (2018) A protocol for combining fluorescent proteins with histological stains for diverse cell wall components. Plant J 93 (2):399-412. doi:10.1111/tpj.13784

Vioque J, Kolattukudy PE (1997) Resolution and purification of an aldehyde-generating and an alcohol-generating fatty acyl-CoA reductase from pea leaves (Pisum sativum L.). Arch Biochem Biophys 340 (1):64-72. doi:10.1006/abbi.1997.9932

Wang Y, Wang M, Sun Y, Hegebarth D, Li T, Jetter R, Wang Z (2015a) Molecular Characterization of TaFAR1 Involved in Primary Alcohol Biosynthesis of Cuticular Wax in Hexaploid Wheat. Plant Cell Physiol 56 (10):1944-1961. doi:10.1093/pcp/pcv112

Wang Y, Wang M, Sun Y, Wang Y, Li T, Chai G, Jiang W, Shan L, Li C, Xiao E, Wang Z (2015b) FAR5, a fatty acyl-coenzyme A reductase, is involved in primary alcohol biosynthesis of the leaf blade cuticular wax in wheat (Triticum aestivum L.). J Exp Bot 66 (5):1165-1178. doi:10.1093/jxb/eru457

Xue D, Zhang X, Lu X, Chen G, Chen ZH (2017) Molecular and Evolutionary Mechanisms of Cuticular Wax for Plant Drought Tolerance. Front Plant Sci 8:621. doi:10.3389/fpls.2017.00621

Zamski E, Shoham O, Palevitch D, Levy A (1987) Ultrastructure of Capsaicinoid-Secreting Cells in Pungent and Nonpungent Red-Pepper (Capsicum-Annuum-L) Cultivars. Bot Gaz 148 (1):1-6. doi:10.1086/337620

Zhang CL, Wang YX, Hu X, Zhang YL, Wang GL, You CX, Li YY, Hao YJ (2020) An apple AP2/EREBP-type transcription factor, MdWRI4, enhances plant resistance to abiotic stress by increasing cuticular wax load. Environ Exp Bot 180. doi:10.1016/j.envexpbot.2020.104206

610 **FIGURE LEGENDS**

611 **Fig. 1** Morphological characteristics of Taiwan oil millet plant. **a** Full image of a 3-month-old plant. **b** Closer
612 image of conspicuous white powder present in the leaf sheath (closed arrow) and pseudopetiole (open arrow).
613 The leaf blade is also indicated (arrowhead). Scale bars: **a** = 10 cm, **b** = 1 cm.

614

615 **Fig. 2** Characteristic features of leaf blade in Taiwan oil millet. **a** Light micrograph of transverse section leaf
616 blade stained with Toluidine Blue showing sclerenchyma cell (arrowhead), bulliform-like cell (asterisk, green),
617 and intercellular space (diamond). One, two, three stars refer to first, second with sclerenchyma on its abaxial
618 side, third order of vascular bundles, respectively. AD, adaxial; AB, abaxial. **b** Autofluorescence image of cross-
619 section of leaf blade indicating the presence of chloroplast. AD, adaxial; AB, abaxial. **c** The adaxial surface of
620 leaf blade micrograph stained with Safranin O and Fast Green. Alternate silica cell (open arrow) and cork cell
621 (closed arrow), including bristle or prickle hair (a hook-type trichome with swollen round base and pointed tip;
622 arrowhead), are present on the line above the major vein. **d**-**e** SEM micrographs of adaxial leaf blade surface.
623 Note the presence of bristle or prickle hair (arrowhead), micro hair (a bottle-shaped bicellular trichome with a
624 larger basal cell and constricted distal cell; open arrow) and filament wax overlapping with the cork cell (closed
625 arrow). AD, adaxial. Scale bars: **a** = 20 μm; **b =** 100 μm; **c**, **d** = 50 μm; **e** = 25 μm.

626

627 **Fig. 3** Characteristic features of Taiwan oil millet leaf sheath. **a** Light micrograph of transverse section of leaf
628 sheath stained with Toluidine Blue depicting sclerenchyma cell (arrowhead) and intercellular space (diamond).
629 AD, adaxial; AB, abaxial. **b** Autofluorescence micrograph of transverse section of leaf sheath showing the red
630 stained chloroplast on the outer abaxial side. AD, adaxial; AB, abaxial. **c** Details of abaxial surface of leaf sheath
631 micrograph stained with Safranin O and Fast Green. Dumbbell-shaped silica cell (open arrow), crenated cork
632 cell (closed arrow), and stomata (arrowhead) are present. **d** Scanning electron microphotograph of outer abaxial
633 leaf sheath showing the extrusion of filament wax from a specific site at the surface (arrowhead) and the
634 presence of micro hairs (double arrow). **e** The inner adaxial of leaf sheath as visualized by SEM displaying the
635 absence of platelet and filament waxes, and the presence of stomata (arrowhead) between long cells. Scale bars:

a = 20 μm; **b, d, e =** 100 μm; **c** = 50 μm.

Fig. 4 Filament wax secretion on the epidermal surface of cork cells in Taiwan oil millet leaf sheath. **a** Newly synthesized wax on the surface of cork cells at 24 h after removal of pre-existing wax could emerge as a single (arrowhead), double (open arrow), linear pores array that eventually encircling (closed arrow) of one cork cell. **b** Freeze-fractured filament wax indicating hollow structure inside. Arrowheads mark the hollow filament wax. **c** Transverse image of leaf sheath merged stained with Nile Red and Calcofluor White. Arrowhead marks the position of papillae on the cork surface. **d** Transverse section of cork cell. Arrowhead marks the papillae protrusion in the cork surface. There are two kinds of cork cell wall: inner (asterisk) and outer (diamond), with dark layer (triangle) on top. **e** Spherical structures (closed arrow) along the inner cork cell wall. There are three layers above the cork plasma membrane: inner (asterisk), outer (diamond) and top darkest layer (triangle). Scale bars: **a** = 25 μm; **b =** 2 μm**; c** = 10 μm; **d =** 1 μm; **e =** 200 nm.

Fig. 5 Wax composition analysis of various tissues of Taiwan oil millet. Percentage of total wax component in the leaf blade (**a**), midrib (**b**), leaf sheath (**c**), pseudopetiole (**d**), and brushed wax (**e**). Total wax load of these 5 parts (**f**); unit: μg cm^{-2} (left y-axis); note the brushed wax unit is μg mg^{-1} dry weight (right y-axis).

Figure 1

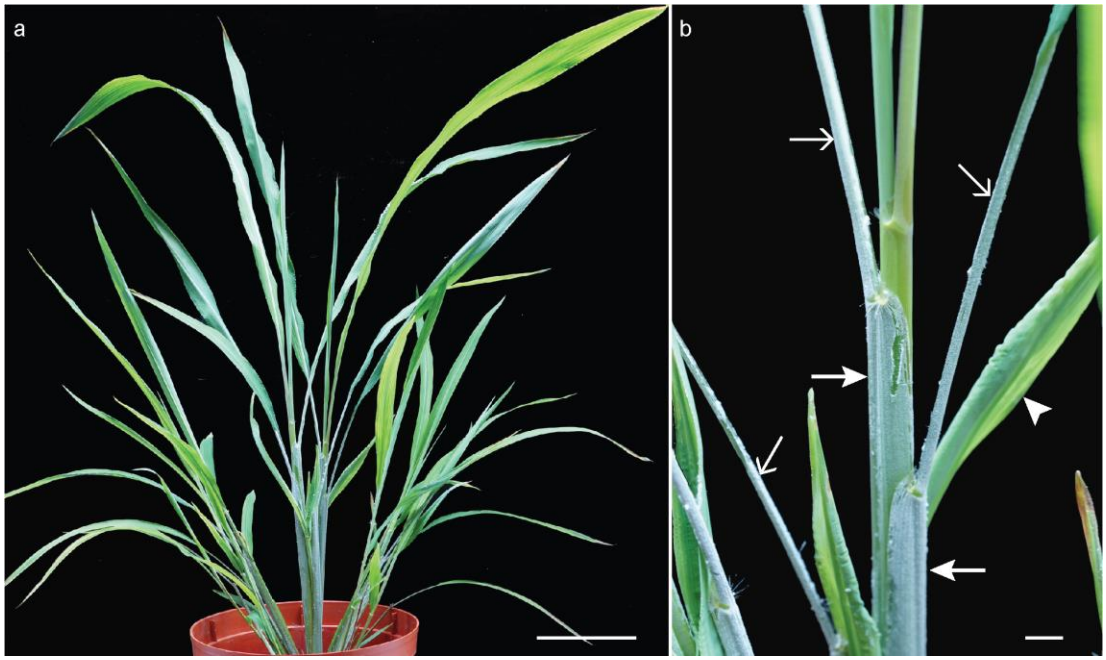

Figure 2

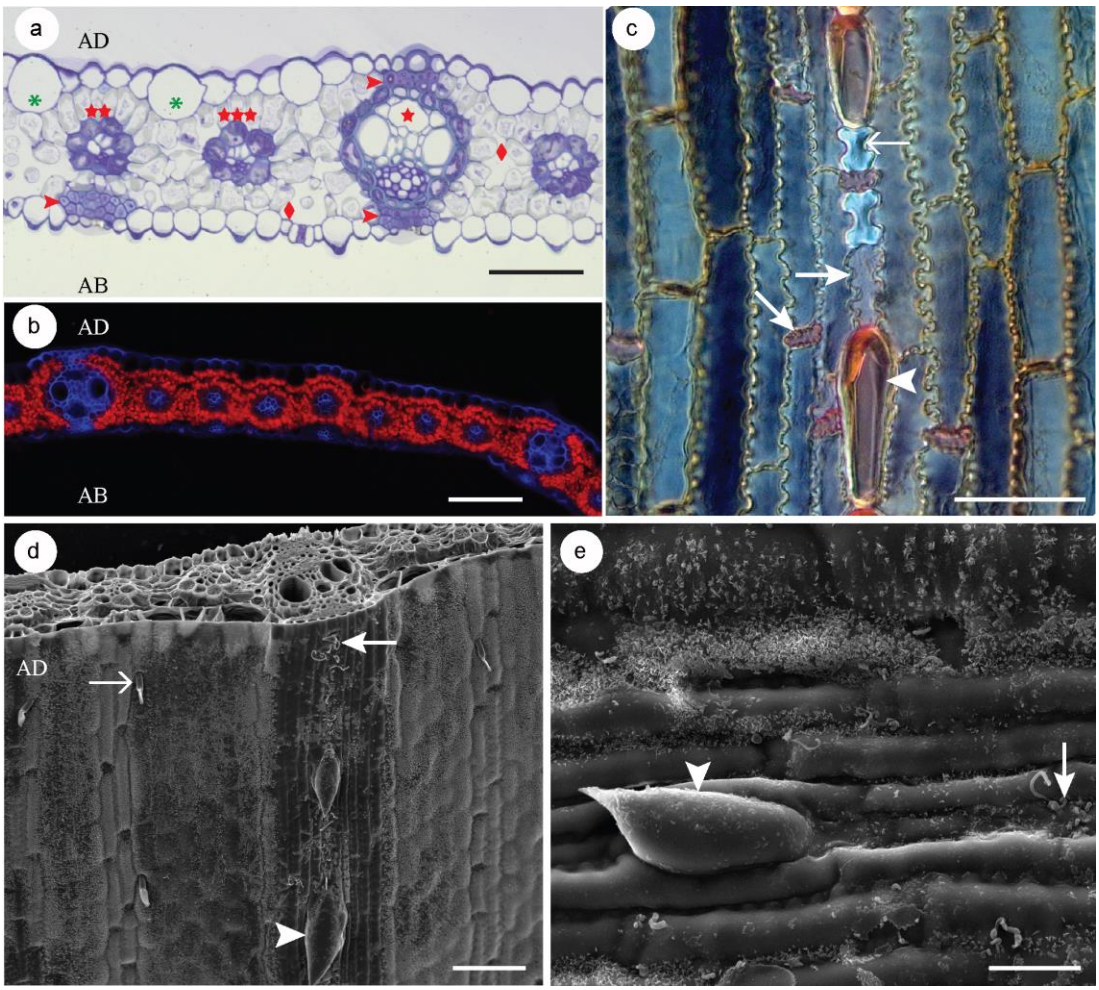

Figure 3

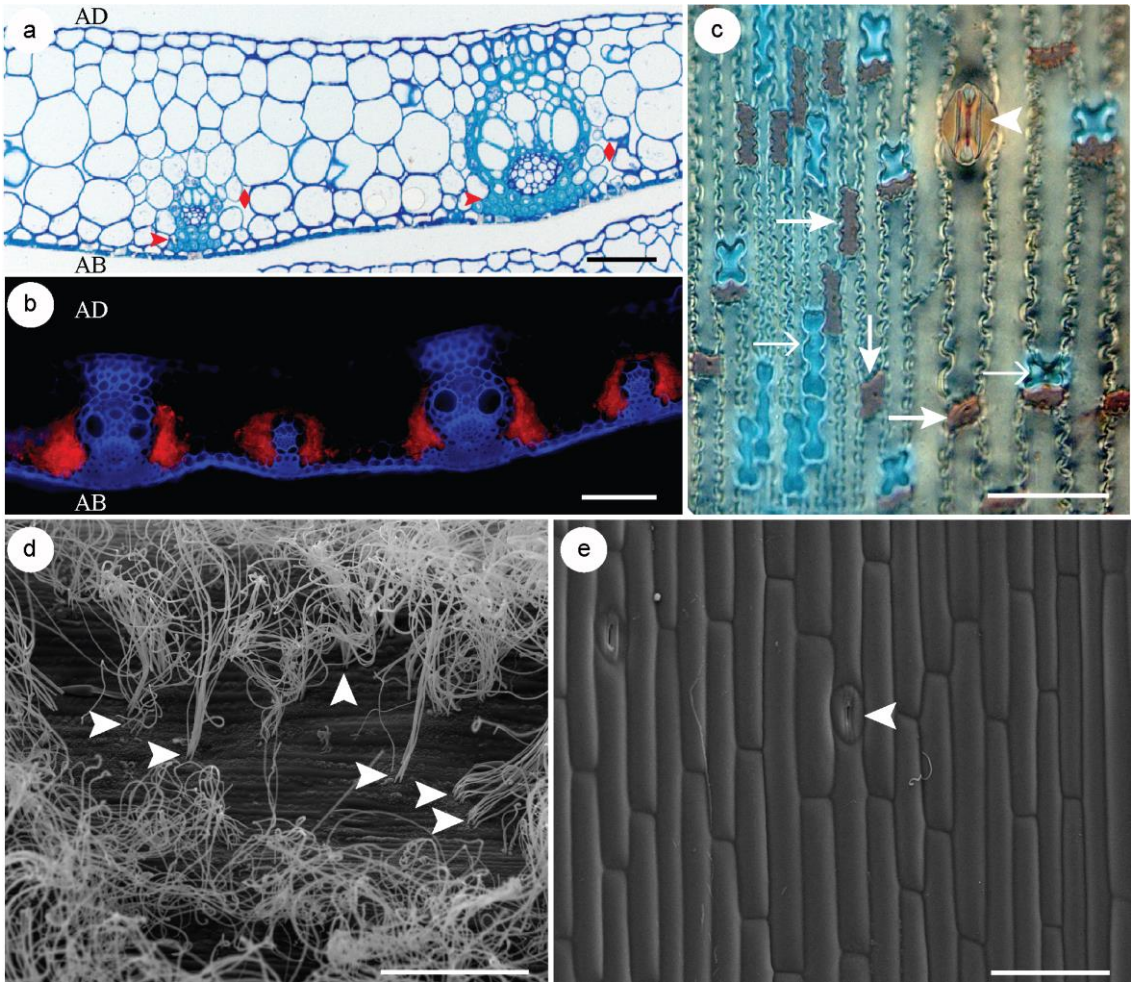

Figure 4

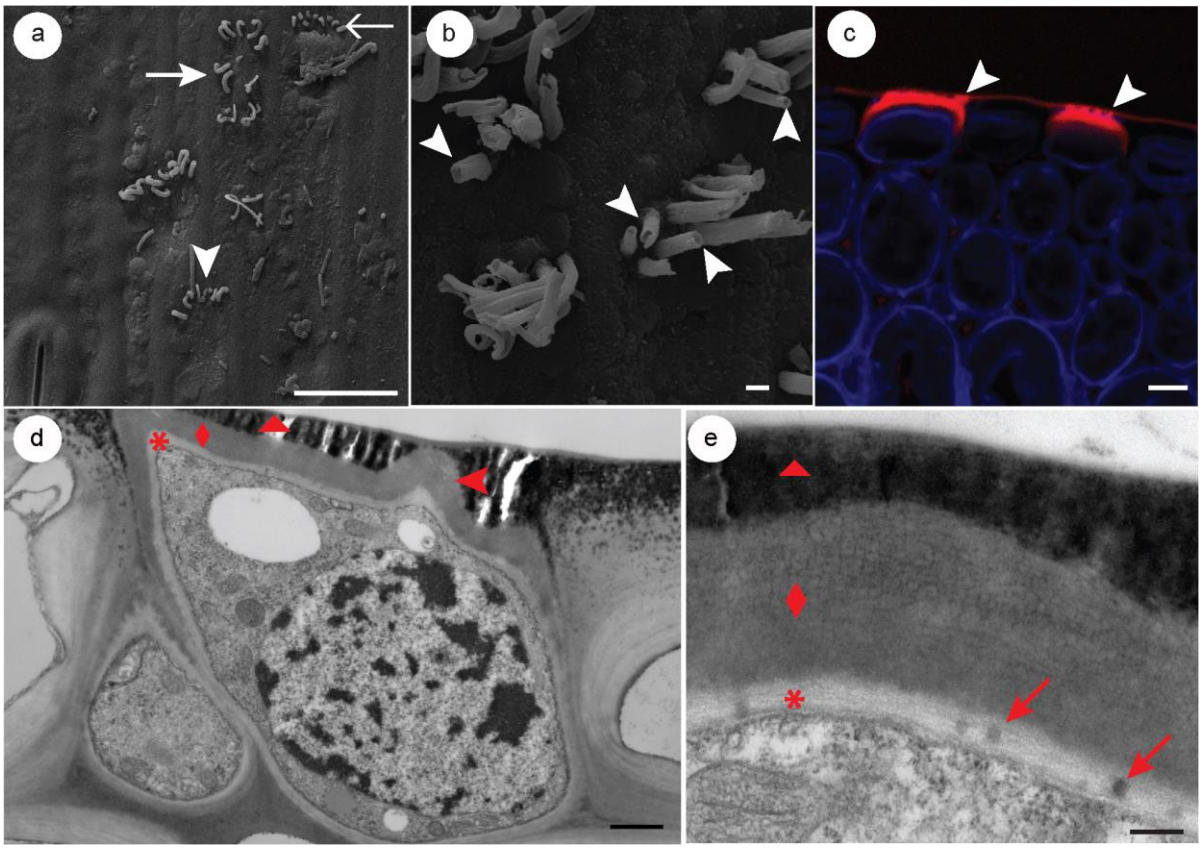

Figure 5

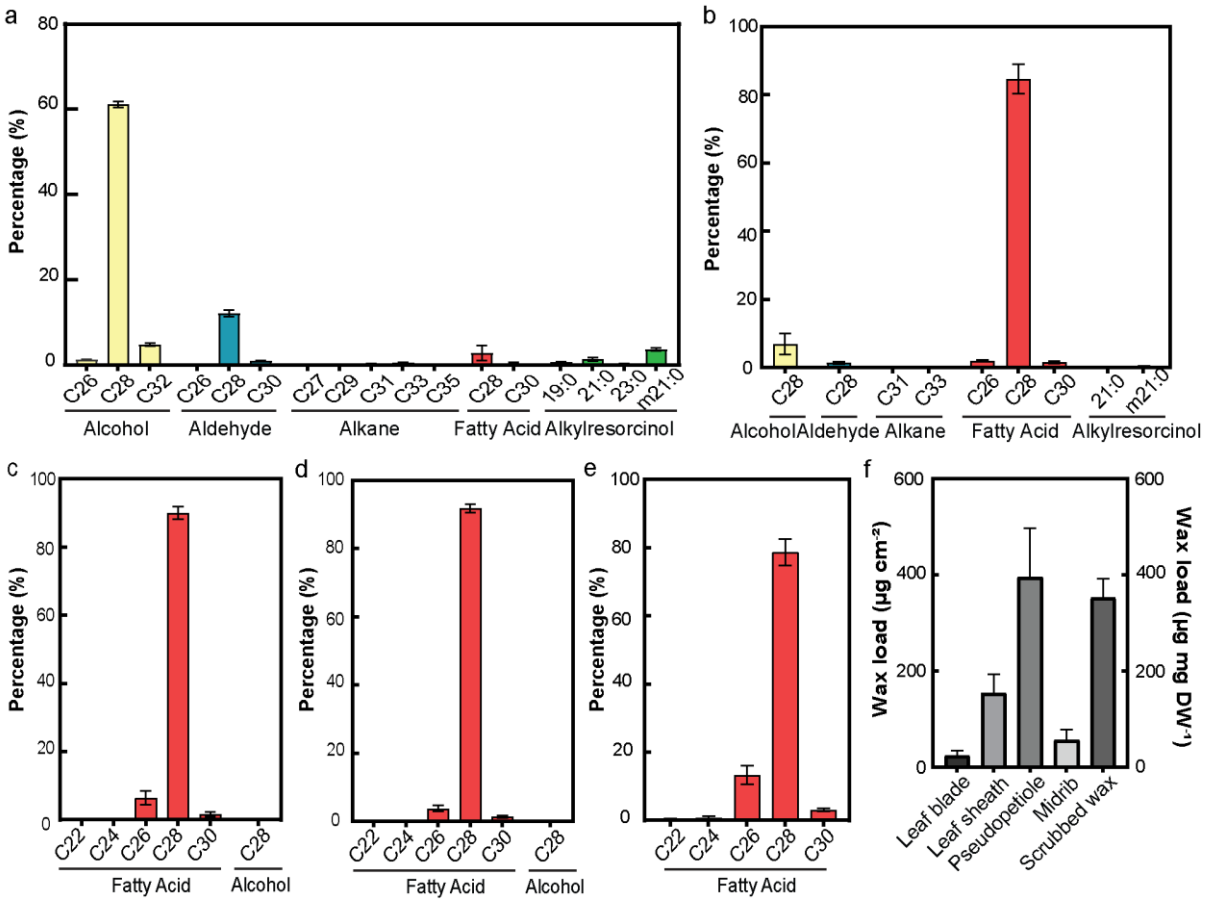
a
Percentage (%)
C26 C28 C32 C26 C28 C30 C27 C29 C31 C33 C35 C28 C30 19:0 21:0 23:0 m21:0
Alcohol
Aldehyde
Alkane
Fatty Acid
Alkylresorcinol
b
Percentage (%)
C28 C28 C31 C33 C26 C28 C30 21:0 m21:0
Alcohol
Aldehyde
Alkane
Fatty Acid
Alkylresorcinol
c
Percentage (%)
C22 C24 C26 C28 C30 C28
Fatty Acid
Alcohol
d
Percentage (%)
C22 C24 C26 C28 C30 C28
Fatty Acid
Alcohol
e
Percentage (%)
C22 C24 C26 C28 C30
Fatty Acid
f
Wax load (μg cm-2)
Wax load (μg mg DW-1)
Leaf blade
Leaf sheath
Pseudopetiole
Midrib
Scrubbed wax